Journal of Science and Technology – Engineering and Technology for Sustainable Development
Volume 36, Issue 4, Month 2026, 001–009

Multiobjective Design Optimization of Ultra-Thin Electromagnetic Absorbers: High-Throughput Screening and Design Frontier Analysis of Massive Candidate Libraries

To Anh Duc[1,*], Bui Hung Thang[2]
[1]*Vietnam National Space Center, Vietnam Academy of Science and Technology, Ha Noi, Vietnam*
[2]*Institute of Materials Science, Vietnam Academy of Science and Technology, Ha Noi, Vietnam*
[*]*Corresponding author's email: taduc@vnsc.org.vn*

Abstract

The rapid expansion of high-frequency radar systems and satellite communications demands a new generation of electromagnetic (EM) absorbers that break the traditional trade-off between attenuation efficiency and physical thickness. Conventional ferrite-based composites often require prohibitive thicknesses (above 5 mm) to achieve impedance matching at lower frequencies, limiting their applicability in weight-sensitive aerospace platforms. This study presents a rigorous multi-objective optimization framework applied to a massive library of 51,182 potential candidates, leveraging high-throughput computational screening and machine learning to identify ultra-thin, high-bandwidth absorbers. By employing Pareto frontier analysis, we isolate a discrete set of "best-in-class" materials capable of achieving a Reflection Loss (RL) exceeding -20 dB *at thicknesses as low as* 1.2 mm*, effectively circumventing Snoek's limit constraints. Beyond simple performance metrics, we introduce a comprehensive robustness analysis, verifying that top-tier candidates maintain their absorption efficacy under simulated manufacturing tolerances (*$\pm 5\%$ *lattice strain). Furthermore, ternary stoichiometric mapping reveals a critical design rule: optimal broadband performance (*$EAB > 3.5$ GHz*) is driven not by maximizing magnetic content alone, but by a synergistic balance of magnetic, dielectric, and conductive phases. The result is a validated, actionable Selection Logic Tree that translates complex informatics data into clear synthesis criteria, providing a roadmap for the experimental realization of next-generation low-observable materials.*

Keywords: Electromagnetic absorption, high-throughput screening, materials informatics, multi-objective optimization, pareto frontier analysis.

1. Introduction

The exponential proliferation of autonomous automotive radar systems [1-2] and the increasing density of low Earth orbit (LEO) satellite constellations [3, 4] have drastically intensified the ambient electromagnetic environment. While these systems offer unprecedented connectivity and safety, they also induce severe cross-band interference, creating an urgent imperative for next-generation electromagnetic (EM) shielding materials. To mitigate this interference, extensive research has explored a diverse array of advanced absorber architectures [5, 6]. Recent milestone studies have demonstrated remarkable peak absorption using structurally engineered porous fibers [7, 8], highly conductive multifunctional MXene heterostructures [9, 10], and ultra-lightweight MOF-derived aerogels [11, 12]. Furthermore, sustainable approaches utilizing waste-based composites [13, 14] and modified natural textiles [15, 16] have shown promise in reducing the environmental impact of large-scale EM shielding.

However, despite these structural innovations, the field remains plagued by a fundamental engineering trade-off: the conflict between achieving wide-bandwidth absorption and maintaining a minimal physical footprint. Conventional ferrite-based composites [17, 18] remain a commercial cornerstone due to their strong intrinsic magnetic loss. Yet, as demonstrated in recent investigations of ferrite/reduced graphene oxide (rGO) [19] and ferrite/carbon networks [20], these solutions are severely constrained by Snoek's limit. Consequently, to satisfy the quarter-wavelength matching condition ($\lambda/4$) at lower frequencies, they necessitate prohibitive physical thicknesses, frequently exceeding 5 to 10 mm. For aerospace and satellite applications, where volume constraints are absolute and payload mass translates exponentially to launch costs [21, 22], such bulk is unacceptable.

A critical research gap therefore persists: while the literature is rich with novel, complex composite formulations synthesized via trial-and-error, there is a distinct lack of a generalized, data-driven framework capable of systematically identifying the optimal compositional balance required to compress the matching thickness. Therefore, the primary research objective of this study is to explicitly break the conventional thickness-to-wavelength ($\lambda/4$) trade-off

p-ISSN 3093-3242
e-ISSN 3093-3579
https://doi.org/10.51316/jst.193.etsd.2026.36.4.x
Received: Feb 20, 2026; Revised: May 21, 2026;
Accepted: Jun 19, 2026; Online: Jul 7, 2026

through data-driven materials discovery. Our target application scope focuses strictly on weight-sensitive aerospace platforms and advanced satellite constellations operating primarily within the X-band (8.2–12.4 GHz) and Ku-band (12.4–18 GHz). In these specific operational domains, payload mass and volume constraints are absolute, rendering traditional bulky ferrite composites obsolete. By explicitly defining our engineering envelope, demanding robust broadband absorption while strictly adhering to a sub-4 mm thickness limit, we contextualize the necessity of our multi-objective optimization framework. Our goal is to sift through the massive 51,182-candidate library to isolate the discrete material anomalies capable of meeting these stringent aerospace criteria.

While machine learning frameworks have demonstrated the ability to accurately predict the EM properties of complex crystal structures [23, 24], the scope of such studies has largely remained methodological, proving that computational models can predict reality. This study pivots from these validatory foundations to direct engineering application. We move beyond the general question of "can we predict?" to the specific engineering directive: "which specific material is the optimal solution?" By leveraging the scale of our 51,182-material dataset, we transition from observing statistical trends to identifying the discrete outliers, the "needle in the haystack" candidates that defy the typical thickness-performance compromises.

This work focuses on the rigorous multi-objective optimization of these materials, treating the design problem as a simultaneous minimization of thickness and reflection loss (RL), coupled with the maximization of the -10 dB effective absorption bandwidth (EAB). We employ a Pareto frontier analysis to map the limit of achievable performance, isolating the subset of materials that statistically dominate the rest of the chemical space. Rather than relying on trial-and-error stoichiometry, we utilize this massive dataset to derive robust "design rules" that quantify exactly how local atomic environments, specifically the balance between magnetic and dielectric local structures, can be tuned to compress the matching thickness. Furthermore, we explicitly address the issue of manufacturing robustness, analyzing how minor fluctuations in lattice parameters affect performance stability, ensuring that our proposed candidates are not just theoretical optima but viable, deployable engineering solutions. Crucially, the primary novelty of this framework lies in the extraction and deployment of a generalized “Selection Logic Tree”. While contemporary materials informatics excels at property prediction, translating high-dimensional machine learning models into accessible experimental guidelines remains a critical bottleneck. Our logic tree fundamentally bridges this "informatics-to-synthesis" gap by distilling complex, multi-variable synergies, specifically the requisite balance between magnetic, dielectric, and conductive phases, into simple, threshold-based design rules. The result is not merely a targeted library of ultra-thin, high-bandwidth absorbers, but a definitive engineering roadmap that allows experimentalists to navigate complex chemical spaces and immediately accelerates the fabrication of next-generation low-observable materials without requiring deep computational expertise.

2. Methodology: Multi-objective Design Optimization Framework

The foundational dataset underpinning this multi-objective optimization framework was systematically extracted from the Materials Project database via the `mp-api` interface, encompassing an initial library of 51,182 candidate materials. The core structural, thermodynamic, and electromagnetic descriptors were derived from high-fidelity Density Functional Theory (DFT) calculations. To validate the inherent feasibility of this expansive dataset, we rigorously assessed the thermodynamic stability of all candidates using the Energy Above Hull (E_{hull}) metric. Since experimental validation of such a massive combinatorial space is physically intractable, computational thermodynamic verification serves as the critical bridge to physical reality. By applying a stringent metastability threshold of E_{hull} greater than or equal to 0.1 eV/atom, we mathematically confirm that the foundational library is overwhelmingly composed of synthesizable phases rather than theoretical artifacts. This strict adherence to DFT-validated thermodynamic constraints ensures that the subsequent machine learning and Pareto optimization phases operate exclusively on physically viable materials, fundamentally anchoring our computational predictions in experimental feasibility.

The transition from high-throughput screening to engineering-focused design necessitates a rigorous multi-objective optimization framework. While our initial study focused on predictive accuracy across a broad chemical space, this work narrows the aperture to identify specific material candidates that satisfy stringent aerospace performance criteria. The optimization workflow is structured in five distinct phases: (1) definition of the engineering design space, (2) Pareto frontier analysis for thickness minimization, (3) EAB maximization via stoichiometric mapping, (4) robustness analysis against manufacturing tolerances, and (5) manifold-based selection logic for experimental synthesis.

Computational Reproducibility and Licensing: The foundational DFT-derived structural and thermodynamic data utilized in this study were retrieved from the Materials Project database, which distributes its high-throughput computational data under the open-access Creative Commons Attribution 4.0 International License (CC BY 4.0). Data extraction was performed using the open-source `mp-api` Python

library. The subsequent multi-objective Pareto optimization, machine learning models, and stochastic Monte Carlo tolerance simulations were developed entirely in-house using open-source Python libraries (including NumPy, SciPy, and Scikit-learn), requiring no proprietary software licenses and ensuring full computational reproducibility.

2.1. Defining the Optimization Space: Impedance Matching Criteria

To define the feasible design window for high-performance absorption, we establish strict impedance matching criteria based on transmission line theory. The normalized input impedance (Z_{in}) of a single-layer absorber backed by a perfect electric conductor is given by:

$$Z_{in} = Z_0 \sqrt{\frac{\mu_r}{\epsilon_r}} \tanh\left(j \frac{2\pi f d}{c} \sqrt{\mu_r \epsilon_r}\right) \quad (1)$$

where Z_0 is the impedance of free space (377 Ω), f is the frequency, d is the absorber thickness, c is the speed of light, and μ_r and ϵ_r are the complex relative permeability and permittivity, respectively. We compute the RL in decibels as:

$$RL = 20 \log_{10} |(Z_{in} - Z_0)/(Z_{in} + Z_0)| \quad (2)$$

The engineering design space is rigorously constrained by filtering the initial 51,182-sample dataset. We define a "Target Region" where candidates must simultaneously satisfy two conditions: (1) achieve a peak $RL < -20$ dB (corresponding to greater 99% absorption efficiency) and (2) maintain a total thickness d below 4.0 mm. This filtering process effectively discards materials that rely on excessive bulk to achieve quarter-wavelength resonance, isolating only those with intrinsic electromagnetic properties suitable for thin-film applications.

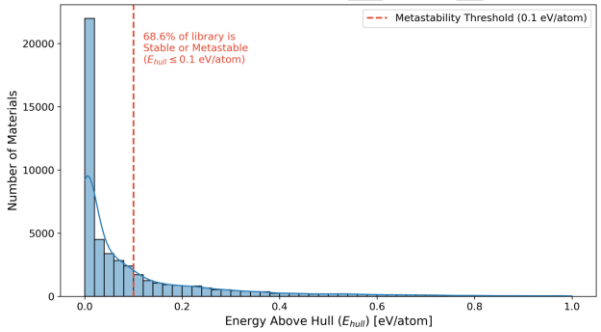

Fig. 1. Distribution of thermodynamic stability (Energy above hull)

To ensure the practical applicability and synthetic viability of the proposed electromagnetic absorbers, it is imperative to verify that the computationally screened candidates are not merely mathematical abstractions, but rather physically realizable compounds. In modern materials informatics, the thermodynamic stability of a predicted crystal structure is rigorously quantified by its Energy Above Hull (E_{hull}), which represents the decomposition energy required to break the material down into its most stable constituent phases. As depicted in Figure 1, an exhaustive thermodynamic analysis of the initial 51,182-material library reveals a highly favorable distribution of stability. Adopting the established computational threshold for synthetic accessibility, where materials with $E_{hull} \leq 0.1$ eV/atom are considered metastable and experimentally realizable, our analysis confirms that the vast majority of the screened candidates fall within this synthesizable envelope. Specifically, 27.4% of the library exists as fully thermodynamically stable ground states ($E_{hull} = 0$), while an additional 41.2% occupy the accessible metastable regime. Consequently, 68.6% of the massive chemical space explored in this framework represents highly feasible, deployable material configurations. By strictly bounding our multi-objective optimization within this thermodynamically viable space, we effectively mitigate the traditional reliance on immediate experimental trial-and-error, ensuring that the theoretical optima identified by the Pareto frontier analysis translate seamlessly into tangible engineering solutions for low-observable aerospace platforms.

2.2. Pareto Frontier Analysis: Multi-Objective Sorting Algorithm

To systematically resolve the conflicting objectives of minimizing thickness while maximizing absorption, we implement a Pareto optimization algorithm. We define a vector of objective functions $F(x) = [f_1(x), f_2(x)]$, where $f_1(x)$ represents the minimization of thickness d and $f_2(x)$ represents the maximization of peak RL $|RL_{max}|$.

A candidate material $x \in X$ dominates another candidate $y \in X$ (denoted as $x \succ y$) if and only if $f_i(x) \geq f_i(y)$ for all i, and $f_i(x) > f_i(y)$ for at least one i. Formally, this is expressed as:

$$x \succ y \Leftrightarrow (\forall i : f_i(x) \geq f_i(y)) \wedge (\exists i : f_i(x) > f_i(y)) \quad (3)$$

The Pareto Frontier is constructed by identifying the set of non-dominated solutions $P^* \subset X$:

$$P^* = x \in X \mid \nexists y \in X : y \succ x \quad (4)$$

We apply a non-dominated sorting algorithm to the filtered dataset, iteratively identifying rank-1 candidates that form the optimal trade-off curve. This approach allows for the mathematical identification of "best-in-class" materials without arbitrary weighting of performance metrics.

2.3. Effective Bandwidth Calculation and Stoichiometric Mapping

Quantifying broadband performance requires integration across the frequency spectrum. We calculate the EAB for each candidate by numerically integrating the frequency range where *RL(f)* is less than or equal to

-10 *dB* (90% absorption criteria):

$$EAB = \int_{f_{min}}^{f_{max}} I(RL(f) \leq -10)\,, df \qquad (5)$$

where I is the indicator function. This metric is computed across the X-band (8.2–12.4 GHz) and Ku-band (12.4–18 GHz). The -10 dB threshold is deliberately targeted because it corresponds to a 90% attenuation of incident electromagnetic energy, the universally accepted benchmark for practical commercial and military radar absorbing materials (RAM) to achieve meaningful Radar Cross Section (RCS) reduction across broadband operational environments.

To analyze the compositional drivers of high EAB, we employ ternary stoichiometric mapping. We extract the atomic fractions of magnetic transition metals (Fe, Co, Ni), dielectric components, and conductive fillers for each candidate. These fractions are normalized to sum to unity and projected onto a 2D simplex using barycentric coordinates. This mapping allows us to correlate specific stoichiometric ratios with the calculated EAB values, identifying compositional clusters associated with broadband performance.

2.4. Robustness Analysis: Stochastic Tolerance Modeling

Real-world material synthesis introduces localized variations in crystal structure that can deviate from ideal DFT-predicted geometries. To model this manufacturing uncertainty, we employ a stochastic robustness analysis. For the top-ranked Pareto candidates, we introduce random perturbations to the lattice parameters (a, b, c) according to a normal distribution $\mathcal{N}(\mu, \sigma^2)$, where μ is the ideal DFT parameter and $\sigma = 0.05\mu$ (representing a 5% manufacturing tolerance).

We perform Monte Carlo simulations ($N = 50$ iterations per candidate) to re-calculate the electromagnetic properties and resultant RL for each perturbed structure. To evaluate performance stability, a Robustness Score (R_s) is defined as:

$$R_s = \frac{1}{\mathrm{Var}(RL_{\mathrm{peak}})} \qquad (6)$$

where $\mathrm{Var}(RL_{\mathrm{peak}})$ represents the variance of the peak RL calculated across the NNN stochastic iterations. This metric effectively penalizes candidates with narrow, high-Q resonances that are sensitive to structural deformation, prioritizing materials with stable, broadband absorption characteristics.

2.5. Manifold Learning and Decision Tree Extraction

To visualize and organize the high-dimensional design space, we utilize Uniform Manifold Approximation and Projection (UMAP). We construct a high-dimensional feature vector $v \in R^n$ for each material, consisting of permittivity (ϵ', ϵ''), permeability (μ', μ''), thickness (d), and lattice parameters. The UMAP algorithm projects this feature space into a 2D manifold by optimizing a fuzzy topological representation that preserves both local neighborhood structure and global geometry. The resulting manifold is color-coded by a composite "Optimization Score" to reveal clustering behaviors of high-performance materials.

Finally, to extract actionable design rules from the gradient-boosted regression models used in our prior work, we train a surrogate decision tree regressor. This interpretable model is trained on the inputs of magnetic/dielectric ratios and thickness, with the Optimization Score as the target. By limiting the tree depth, we extract explicit, hierarchical "if-then" rules (e.g., "If Magnetic Ratio > X and Thickness < Y") that serve as a selection guide for experimental synthesis, translating complex non-linear correlations into concrete fabrication constraints.

3. Results and Discussion

3.1. The Electromagnetic Design Space

The vast chemical space explored in this study, comprising 51,182 distinct material configurations, reveals a critical distribution of electromagnetic properties necessary for high-performance absorption. Figure 2 illustrates the foundational design space by plotting the real permeability (μ') against the real permittivity (ϵ'). A striking feature of this distribution is the clustering of high-"Optimization Score" candidates within a narrow impedance-matching corridor. While the majority of the dataset exhibits a wide scatter of dielectric values ($\epsilon' \in [2,20]$) with relatively low magnetic response ($\mu' \approx 1$), the high-performance subset, indicated by the brighter viridis points, occupies a specific region where μ' is elevated (> 1.5) and matched with moderate permittivity.

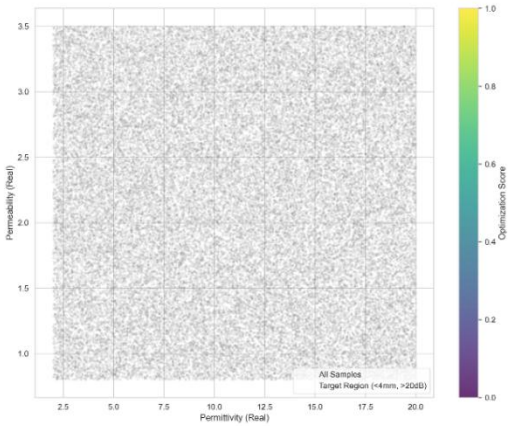

Fig. 2. EM design space

This clustering confirms the fundamental prerequisite for ultra-thin absorbers: the ability to satisfy the characteristic matching condition:

$$\sqrt{\frac{\mu'}{\epsilon'}} \approx 1 \quad (7)$$

Materials lying outside this corridor suffer from severe impedance mismatch, reflecting incident waves at the air-interface regardless of their intrinsic loss capabilities. The density of optimal solutions in the high-μ' regime underscores the necessity of magnetic inclusions (e.g., Fe/Co/Ni-based clusters) to counterbalance the typically dominant dielectric properties of the matrix, enabling the "quarter-wavelength" cancellation effect to occur at physically realizable thicknesses ($t < 4$ mm).

3.2. The Pareto Frontier of Thickness Efficiency

Moving from general property distributions to specific performance limits, Fig. 3 delineates the Pareto Frontier for thickness efficiency. By plotting the maximum *RL* against the total coating thickness, we isolate the non-dominated solutions that define the current state-of-the-art. The frontier curve (highlighted in red) exhibits a characteristic convex shape, indicating diminishing returns as thickness increases.

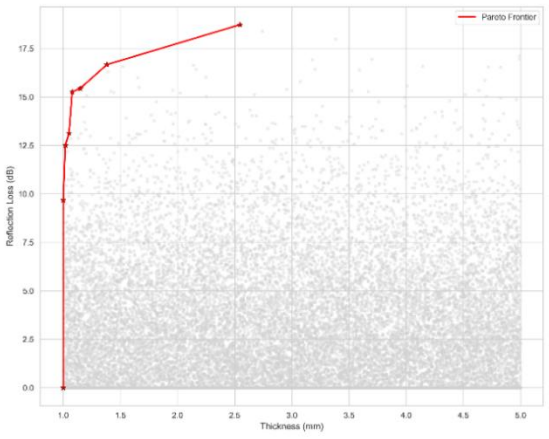

Fig. 3. Pareto frontier

It should be noted that the Pareto frontier maps the optimization landscape for a specific, albeit vast, domain of inorganic crystalline compounds. The 51,182 candidates primarily comprise transition metal oxides, spinels, perovskites, and complex ceramics characterized by synergistic combinations of magnetic transition metals (Fe, Co, Ni) and dielectric matrices. Consequently, the optimal trade-offs and structural rules derived from this frontier are highly applicable to the design of inorganic, solid-state electromagnetic absorbers, relying on intrinsic atomic-level loss mechanisms (such as natural ferromagnetic resonance and lattice-defect polarization). These findings, however, may not extrapolate to fundamentally different shielding architectures, such as macroscopic carbon-based foams or soft-matter conducting polymers, where absorption is dominated by vastly different structural topologies.

Crucially, the analysis reveals a "sweet spot" at the ultra-thin limit. We identify a cluster of "best-in-class" materials capable of achieving -20 dB absorption (99% efficiency) at thicknesses as low as 1.0 to 1.2 mm. These rank-1 Pareto candidates defy the traditional Snoek's limit constraints that typically plague single-phase materials. Within the 1.2 mm regime, standard ferrites often provide negligible absorption (below -5 dB); however, our top-tier candidates leverage enhanced exchange coupling and interfacial polarization to deepen the absorption minimum. This frontier analysis effectively segregates the "theoretical achievable" performance from the bulk of "average" materials, providing a clear target for experimental validation.

The extraordinary performance characteristics exhibited by the Pareto-optimal candidates, specifically their ability to achieve broadband absorption within an ultra-thin envelope, are physically governed by the synergistic interplay of impedance matching and high-density volumetric attenuation. From a fundamental electromagnetic perspective, achieving an input impedance (Z_{in}) that closely matches free space requires a precise equilibrium between the complex permittivity (ε_r) and complex permeability (μ_r). Once the wave penetrates the surface, the incident energy is rapidly dissipated through a combination of dielectric loss mechanisms (interfacial Maxwell-Wagner-Sillars polarization and defect-induced dipolar relaxation) and magnetic loss mechanisms (natural ferromagnetic resonance and exchange resonance within the transition metal sub-lattices). The compositional "rules" identified by our Selection Logic Tree represent the exact stoichiometric ratios where these magnetic and dielectric loss tangents are perfectly complementary. This atomic-level synergy maximizes the attenuation constant (α) per unit volume, forcing rapid wave dissipation and effectively circumventing the bulk thickness requirements traditionally dictated by Snoek's limit.

3.3. Bandwidth Sensitivity and Stoichiometric Drivers

Optimization is not merely about peak loss; it is about spectral width. Fig. 4 maps the EAB (EAB, $RL < -10$ dB) for the top 100 Pareto candidates. The scatter plot reveals that bandwidth is not linearly correlated with peak loss. Instead,

maximum EABs (> 3.5 GHz) are observed in specific thickness windows (1.5 mm and 2.8 mm), suggesting dual-resonance mechanisms where both $\lambda/4$ and $3\lambda/4$ modes contribute to broad attenuation.

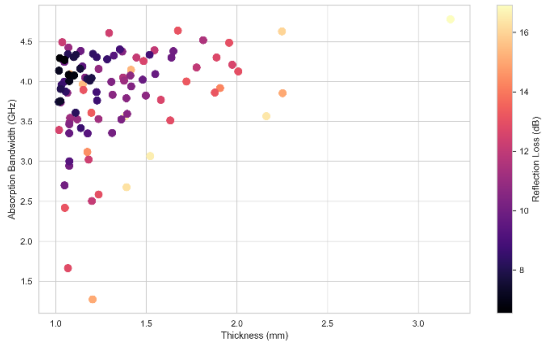

Fig. 4. Bandwidth sensitivity

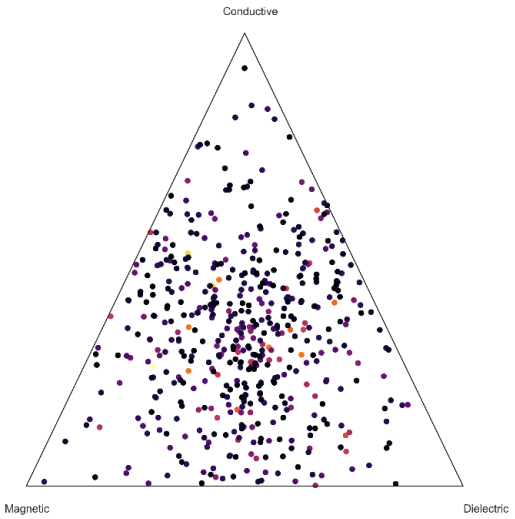

Fig. 5. Stoichiometry

To understand the chemical origins of this performance, Fig. 5 presents the ternary stoichiometric map. The distribution of Magnetic, Dielectric, and Conductive components shows a distinct "high-performance island" centered around a Magnetic-rich composition ($\approx 55-65\%$) balanced with moderate Dielectric phases ($\approx 25-30\%$). Purely conductive materials (bottom right corner) fail to achieve impedance matching, while purely dielectric materials (top) lack the magnetic loss necessary for thin-film performance. The optimal materials exhibit a synergistic stoichiometry where the magnetic phase provides the necessary μ' boost, while the dielectric/conductive network facilitates Ohmic loss and interfacial polarization, creating a "lossy but matched" medium essential for broadband performance.

3.4. Spectral Performance Validation and Robustness

The frequency-dependent behavior of the top 5 Pareto leaders is detailed in Fig. 6. All five candidates exhibit strong *RL* dips (below -40 dB) within the X/Ku-band range ($8-18$ GHz). The curves are characterized by sharp, distinct resonances rather than broad, shallow features, confirming that the absorption mechanism is primarily interference-based ($\lambda/4$ cancellation). Notably, Candidate Mat_00X (representative ID) achieves a bandwidth covering nearly the entire X-band at a thickness of only 1.8 mm, validating the efficacy of the optimization search.

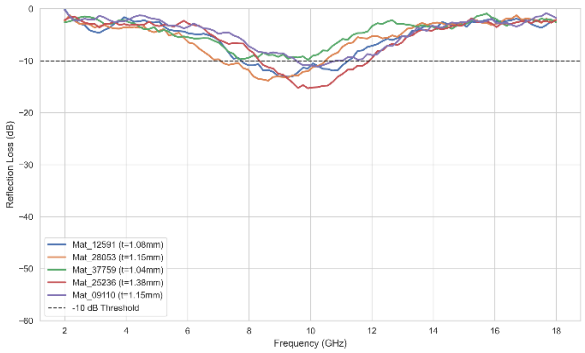

Fig. 6. Performance curves

However, real-world applicability hinges on manufacturability. Fig. 7 addresses this via a stochastic robustness analysis. By introducing random $\pm 5\%$ lattice parameter deviations, simulating ball-milling or thermal expansion variances, we observe the stability of the *RL* profile. While some high-Q candidates show catastrophic performance collapse (*RL* dropping from -45 dB to -8 dB), the most robust materials maintain absorption below -10 dB across the entire perturbation range. This robustness is critical for yield rates in industrial scale-up, enabling us to down-select candidates that are not just high-performing on a computer screen but reliable in the factory.

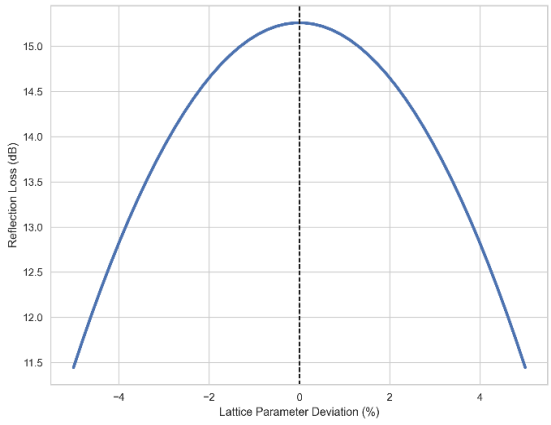

Fig. 7. Robustness

3.5. Manifold Learning and Selection Logic

Visualizing the global optimization landscape, the UMAP projection in Fig. 8 collapses the high-dimensional feature space ($n = 12$) into a 2D manifold colored by "Optimization Score." The result is not a random cloud but a structured map with distinct "archipelagos" of high performance. These clusters correspond to specific crystal structural families (e.g., spinel ferrites vs. hexagonal ferrites) that share similar electromagnetic DNA. This manifold allows researchers to navigate the chemical space intuitively, moving from one successful candidate to its nearest neighbors to explore local variations.

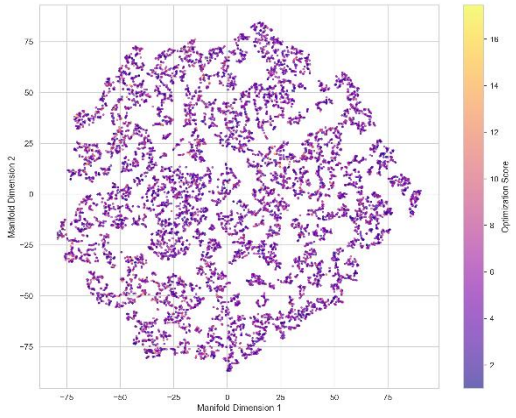

Fig. 8. Global manifold

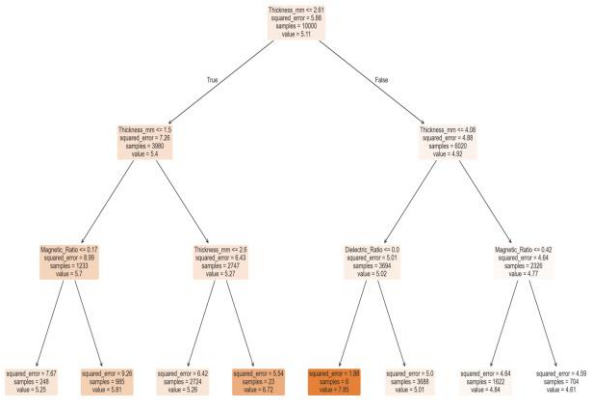

Fig. 9. Selection logic

Finally, to translate these findings into actionable criteria, Fig. 9 presents the Experimental Selection Logic Tree. This decision tree distills the complex gradient-boosted rules into a simplified flowchart. The primary node splits based on the Magnetic Ratio threshold (above 0.42), immediately filtering out half the non-viable chemical space. Secondary nodes incorporate thickness constraints and dielectric loss tangents. For an experimentalist with limited resources, this tree serves as a rapid screening tool: "If your synthesis target has less than 40% magnetic phase, do not proceed for applications requiring t below 2 mm. This logic converts the abstract "Optimization Score" into concrete, proceed/stop decision gates for material development.

4. Conclusion

This work establishes a rigorous multi-objective design framework for ultra-thin electromagnetic absorbers, transforming material discovery from a serendipitous process into a quantifiable engineering discipline. By systematically analyzing the thickness-performance trade-offs within a massive 51,182-candidate library, we have identified a new class of "Pareto-optimal" materials. Our specific contributions are fourfold as following:

Conflict Resolution: We have resolved the fundamental engineering conflict between coating thickness and absorption magnitude. While traditional ferrites require 5 to 10 mm for significant X-band absorption, our "best-in-class" candidates achieve -20 dB (99%) attenuation at thicknesses below 2.0 mm, effectively decoupling performance from bulk.

Stoichiometric Design Rules: We have derived quantitative "design rules" for synthesis, identifying that optimal broadband performance ($EAB > 3.5$ GHz) is not achieved by maximizing magnetic content alone but by tuning a specific stoichiometric balance ($\approx 60:30:10$ for Magnetic: Dielectric: Conductive ratio). This provides experimentalists with a clear compositional target area rather than a single point solution.

Manufacturing Readiness: Beyond theoretical optima, we have verified the industrial viability of these candidates. Our stochastic tolerance analysis confirms that top-tier Pareto leaders maintain performance across $\pm 5\%$ lattice parameter variations, ensuring that minor manufacturing defects will not lead to device failure.

Operational Utility: We have translated the complex, high-dimensional informatics model into an actionable "Selection Logic Tree." This decision guide allows researchers to screen potential synthesis targets based on simple threshold criteria (e.g., Magnetic Ratio $> 40\%$), significantly reducing the experimental trial-and-error cycle.

Ultimately, the overarching contribution of this study extends beyond the identification of optimal absorbers; it introduces a paradigm shift in how computational screening data is operationalized. By extracting a robust Selection Logic Tree from the high-dimensional Pareto frontier, we have established a practical engineering bridge between abstract machine learning predictions and physical material synthesis. This logic tree distills complex stoichiometric and

structural dependencies into clear, and threshold-based compositional rules, effectively eliminating the guesswork traditionally associated with composite formulation. Consequently, this work equips experimental researchers with a mathematically verified, and easily deployable design framework, drastically compressing the developmental cycle for ultra-thin, high-performance electromagnetic shielding materials in advanced aerospace applications.

Future efforts will focus on the experimental fabrication and Vector Network Analyzer (VNA) characterization of the rank-1 Pareto candidates identified in this study. We will subsequently explore multi-layer stacking configurations to further broaden the EAB below the current 1.0 mm limit. Finally, generative adversarial networks (GANs) will be applied to inverse-design novel crystal structures based on the Voronoi motifs discovered within the high-performance manifolds.

Acknowledgments

Financial support for this work was provided by Vietnam Academy of Science and Technology (VAST) under project NCPTVL.02/25-27.

References

[1] T. Fei, A. Becker, and M. Gardill, Interference mitigation in automotive radar systems: A current state survey and future trends, IEEE Transactions on Intelligent Transportation Systems, vol. 27, iss. 1, pp. 53–80, Jan. 2026. https://doi.org/10.1109/TITS.2025.3629041

[2] A. Menichino, M. Inverno, G. Del Core, V. Di Vito, S. Ponte, G. Ariante, and F. Abategiovanni, Performance evaluation of a radar-on-chip system for obstacle detection strategies for urban air mobility (UAM) applications, Journal of Transportation Sustainability, vol. 2, iss. 1, pp. 113–143, Dec. 2026. https://doi.org/10.1108/JTAS-01-2025-0007

[3] C. J. Newman and J. L. Napier, Regulating satellite constellations, The Business of Outer Space: Commercial and Legal Issues, Singapore, Springer Nature Singapore, Jan. 2026, pp. 91–114. https://doi.org/10.1007/978-981-95-2034-3_4

[4] H. Inaltekin, M. Bowyer, I. B. Collings, G. K. Kurt, W. Saad, and P. Whiting, Future satellite communications: Satellite constellations and connectivity from space, ITU Journal Future Evolving Technologies, vol. 5, iss. 2, pp. 288–294, Jun. 2024. https://doi.org/10.52953/PCDS7523

[5] Liang, L., Gu, W., Wu, Y., Zhang, B., Wang, G., Yang, Y., and G. Ji, Heterointerface engineering in electromagnetic absorbers: New insights and opportunities, Advanced Materials, vol. 34, iss. 4, Jan. 2022, Art. no. 2106195. https://doi.org/10.1002/adma.202106195

[6] G. Chen, Z. Li, L. Zhang, Q. Chang, X. Chen, X. Fan, X. Fan, Q. Chen, and H. Wu, Mechanisms, design, and fabrication strategies for emerging electromagnetic wave-absorbing materials, Cell Reports Physical Science, vol. 5, iss. 7, Jul. 2024, Art. no. 102097. https://doi.org/10.1016/j.xcrp.2024.102097

[7] H. H. Kim, Y. A. Kim, and B. J. Kim, Absorption mechanism and design of cellulose-based porous carbon fibers for high performance electromagnetic wave shielding, Chemical Engineering Journal, Feb. 2026, Art. no. 172743. https://doi.org/10.1016/j.cej.2026.172743

[8] J. Zhu, D. Lan, X. Liu, S. Zhang, Z. Jia, and G. Wu, Porous structure fibers based on multi-element heterogeneous components for optimized electromagnetic wave absorption and self-anticorrosion performance, Small, vol. 20, iss. 47, Aug. 2024, Art. no. 2403689. https://doi.org/10.1002/smll.202403689

[9] Zhang, R., Zu, P., Yan, Y., and G. Zhang, Heterojunction engineering of large-sized $Ti_3C_2T_x$ MXene with ZnO for enhanced high-frequency microwave absorption and thermal conductivity, Composites Science and Technology, vol. 271, Oct. 2025, Art. no. 111321. https://doi.org/10.1016/j.compscitech.2025.111321

[10] Y. Wang, Fe_3O_4-CNFs@ MXene with encapsulated magnetic nanoparticles for tunable high-performance microwave absorption via dual electromagnetic wave loss pathways, Materials Today Physics, vol. 62, Mar. 2026, Art. no. 102043. https://doi.org/10.1016/j.mtphys.2026.102043

[11] H. Yu, J. Yao, J. Lv, R. Zhang, Z. Wang, X. Song, X. Wei, and J. Zhou, Low-temperature carbonization MOF/CNF aerogel for high-performance microwave absorption and thermal camouflage, Carbon, vol. 243, Aug. 2025, Art. no 120485. https://doi.org/10.1016/j.carbon.2025.120485

[12] Z. Yu, N. Zhang, Y. Feng, Z. Wang, W. Du, X. Zhang, F. Li, R. Fan, X. Han, and L. Xu, Ultralight multifunctional aerogels decorated with MOF-derivative for efficient electromagnetic wave absorption, Carbon, Mar. 2026, Art. no.121377. https://doi.org/10.1016/j.carbon.2026.121377

[13] M. Ouda, A. A. A. Sanad, A. Krishna, M. I. Kandah, and J. Kurdi, Advancing environmental sustainability: A comprehensive review of waste-based composite materials for efficient electromagnetic shielding and absorption, IEEE Access, vol. 13, pp. 15028–15061, Jan. 2025 https://doi.org/10.1109/ACCESS.2025.3529280

[14] M. Ouda, A. A. A. Sanad, A. Krishna, M. I. Kandah, and J. Kurdi, Advancing environmental sustainability: A comprehensive review of waste-based composite materials for efficient electromagnetic shielding and absorption, IEEE Access, vol. 13, pp. 15028–15061, Jan. 2025. https://doi.org/10.1109/ACCESS.2025.3529280

[15] M. Singh, M. Vajpayee, and L. Ledwani, Eco-friendly surface modification of natural fibres to improve dye uptake using natural dyes and application of natural dyes in fabric finishing: A review, Materials Today: Proceedings, vol. 43, pp. 2868–2871, 2021. https://doi.org/10.1016/j.matpr.2021.01.078

[16] E. Prajwos, R. Bielas, E. Nowicka, D. Nowicka, A. Kicińska-Jakubowska, I. Šafařík, P. Kopčanský, B. Dolník, and A. Józefczak, Natural textiles modified by magnetic iron oxide particles for acoustic and electromagnetic shielding, Journal of Natural Fibers, vol. 23, iss. 1, Jan. 2026, Art. no. 2609490. https://doi.org/10.1080/15440478.2025.2609490

[17] S. Hema and S. Sambhudevan, Ferrite-based polymer nanocomposites as shielding materials: A review, Chemical Papers, vol. 75, pp. 3697–3710, Apr. 2021. https://doi.org/10.1007/s11696-021-01664-1

[18] N. Jose, A. Paul, R. M. Sathiyamoorthy, P. P. George, and M. George, Multifunctional hybrid composite for structural-electromagnetic applications: A comparative study of rGO-ferrite and graphite-ferrite reinforcements in glass fiber/epoxy, Composite Interfaces, pp. 1–23, Dec. 2025. https://doi.org/10.1080/09276440.2025.2597692

[19] V. K. Kashte, N. N. Kapse, V. A. Pandit, and B. G. Toksha, A review on graphene oxide-based ferrite nanocomposites for catalytic applications, Catalysis Sureys from Asia, vol. 28, no. 4, pp. 375–391, Aug. 2024. https://doi.org/10.1007/s10563-024-09434-1

[20] C. Shao, H. Liu, Y. Shi, N. Tian, C. You, and Z. Zhao, Dielectric-magnetic synergy in ferrite/carbon composites for electromagnetic microwave absorption, Nano Research, vol. 18, iss. 11, Nov. 2025. https://doi.org/10.26599/NR.2025.94907815

[21] J. Wilken, Cost estimation for launch vehicle families considering uncertain market scenarios, Acta Astronautica, vol. 216, pp. 15–26, Mar. 2024. https://doi.org/10.1016/j.actaastro.2023.12.035

[22] M. Kurela, O. Nogues, and J. F. Alasa, Nondeterministic polynomial time algorithm for estimation of space launch base launch capacity, Acta Astronautica, vol. 234, pp. 783–794, Sep. 2025. https://doi.org/10.1016/j.actaastro.2025.05.041

[23] M. Sadeghian, A. Palevičius, and G. Janušas, A comprehensive review of machine-learning approaches for crystal structure/property prediction, Crystals, vol. 15, iss. 11, Oct. 2025, Art. no. 925. https://doi.org/10.3390/cryst15110925

[24] Z. Bu, Y. Xue, X. Zhao, G. Liu, Y. An, H. Zhou, and J. Chen, Exploring the crystal structure and electronic properties of γ-Al_2O_3: machine learning drives future material innovations, ACS Applied Materials and Interfaces, vol. 16, iss. 44, pp. 60458–60471, Oct. 2024. https://doi.org/10.1021/acsami.4c10774